Biosensors and Bioelectronics 85 (2016) 625–632

Contents lists available at ScienceDirect

Biosensors and Bioelectronics

journal homepage: www.elsevier.com/locate/bios

Visual and fluorescent assays for selective detection of beta-amyloid oligomers based on the inner filter effect of gold nanoparticles on the fluorescence of CdTe quantum dots

Ning Xia, Binbin Zhou, Nanbing Huang, Mengsha Jiang, Jiebing Zhang, Lin Liu *

Key Laboratory of New Optoelectronic Functional Materials (Henan Province), College of Chemistry and Chemical Engineering, Anyang Normal University, Anyang, Henan 455000, People's Republic of China

ARTICLE INFO

Article history:
Received 16 April 2016
Received in revised form
20 May 2016
Accepted 21 May 2016
Available online 24 May 2016

Keywords:
Beta-amyloid
Inner filter effect
Fluorescent biosensor
Visual assay
Quantum dots
Gold nanoparticles

ABSTRACT

Beta-amyloid (Aβ) peptides are the major constituents of senile plaques in the brains of Alzheimer's disease (AD) patients. Aβ monomers (AβMs) can coalesce to form small, soluble oligomers (AβOs), followed by reorganization and assembly into long, thread-like fibrils (AβFs). Recently, soluble AβOs have been regarded as reliable molecular biomarkers for the diagnosis of AD because of their high toxicity for neuronal synapse and high concentration levels in the brains of AD patients. In this work, we reported a label-free, sensitive and selective method for visual and fluorescent detection of AβOs based on the inner filter effect (IFE) of gold nanoparticles (AuNPs) on the fluorescence of CdTe quantum dots (QDs). Specifically, the fluorescence of CdTe QDs was quenched significantly by AuNPs through the IFE. PrP(95–110), an AβOs-specific binding peptide from cellular prion protein, triggered the aggregation and color change of AuNPs suspension; thus, the IFE of AuNPs on the fluorescence of CdTe QDs was weakened and the fluorescence intensity was recovered. However, in the presence of AβOs, the specific interaction of AβOs and PrP(95–110) prevented the absorption of PrP(95–110) onto the surface of AuNPs. As a result, the aggregation of AuNPs was inhibited and the fluorescence intensity of CdTe QDs was quenched again. This label-free method is specific for detection of AβOs but not for AβMs and AβFs. The detection limits were found to be 0.5 nM for the visual assay and 0.2 nM for the fluorescent detection. We believe that this work would be valuable for many investigations related to AD diagnosis and drug discovery.

1. Introduction

Alzheimer's disease (AD) accounts for 60–70% of cases of dementia and affects approximately 48 million people worldwide in 2015. The two neuropathological hallmarks of AD are the accumulation of intracellular neurofibrillary tangles of abnormally phosphorylated microtubule-associated protein tau and extracellular senile plaques composed primarily of beta-amyloid (Aβ) peptides including 39–42 amino acid residues (Rauk, 2009). Aβ monomers (AβMs) in their native form are normally secreted, soluble, proteolytic cleavage products from amyloid precursor protein (APP) by β- and γ-secretase. However, they can coalesce to form small, soluble oligomers (AβOs) comprised of 50–100 AβMs, followed by further reorganization and assembly into long, insoluble, and often twisted, thread-like fibrils (AβFs). Thus, AβMs or AβOs have been regarded as the reliable molecular biomarkers and therapeutic targets for the diagnosis and prognosis of AD (Kaushik et al., 2016; Xing and Xia, 2015).

Recently, a few novel techniques have been developed to probe for AβMs, such as electrochemistry (Escosura-Muñiz et al., 2015; Liu et al., 2014a, 2013; Yu et al., 2015, 2014), surface plasmon resonance (SPR) (Xia et al., 2010), microassay (Gagni et al., 2013), resonance lights scattering (Wang et al., 2011) and gold nanoparticle-based dot-blot immunoassay (Wang et al., 2012). However, assays measuring AβMs might be unable to discriminate between AD patients and healthy controls or other types of dementia, because the levels of AβMs may differ by gender and age (Golde et al., 2000). Additionally, some of these methods require the utilization of expensive and less stable antibodies to capture and recognize AβMs, and the use of AβMs antibody as a bioreceptor would also recognize Aβ aggregates as well as its metabolites to some extent in patient samples. Thus, these methods for clinically detecting AβMs have inherent shortcomings in that they are expensive, labor-intensive and less specific. It has been suggested that soluble AβOs are capable of diffusing in the neuropil, potentially more neurotoxic than amyloid plaques, and likely responsible for the synaptic dysfunction and memory loss in AD patients and AD animal models (Xing and Xia, 2015). Several observations have also documented that AβOs possess ligand-like

* Corresponding author.
E-mail address: liulin@aynu.edu.cn (L. Liu).

http://dx.doi.org/10.1016/j.bios.2016.05.066
0956-5663/

properties. For example, they can bind to neurons with high affinity and specificity and trigger distinct cellular signal transduction responses, culminating in synaptic dysfunction and neuronal death (Glabe, 2008; Walsh et al., 2002). Furthermore, the concentration of soluble AβOs correlates with synapse loss and memory deficit in humans as well as in AD mouse models, and the introduction of exogenous AβOs can induce memory deficits in rodents (Haes et al., 2005; Reinke et al., 2010; Selkoe, 2008). In this context, the direct determination of neurotoxic AβOs would be more reliable for the AD diagnosis than that by detection of AβMs. Therefore, it is highly desirable to develop a simple, sensitive and selective method for the detection of ultra-low concentrations of AβOs.

It has been suggested that cellular prion protein (PrP^C) is a natural, neuronal receptor that binds specifically to AβOs but not AβMs and AβFs (Balducci et al., 2010; Freir et al., 2011; Laurén et al., 2009). Several studies have demonstrated that the core region of PrP^C for the AβOs/PrP^C interaction is PrP(95–110) (Balducci et al., 2010; Chen et al., 2010; Fluharty et al., 2013; Guillot-Sestier et al., 2012), which is located within the unstructured N-terminal region of PrP^C with an amino acid sequence of THSQWNKPSKPKTNMK. In the present work, we found that PrP (95–110) could induce the aggregation and color change of gold nanoparticles (AuNPs), whereas the formation of AβOs-PrP(95–110) prevented the PrP(95–110)-triggered AuNPs aggregation. The findings give us a hint that the specific interaction between AβOs and PrP(95–110) could be exploited in the development of a simple and selective visual biosensor for AβOs detection. Moreover, although AuNPs-based colorimetric assays have been widely applied in various fields because of the simple manipulation principle and easy procedure for signal readout, the majority of colorimetric assays exhibit poor sensitivity (Elghanian et al., 1997; Liu et al., 2012). We suggest that the above examples could be re-creations of the existing platforms for achieving new goals, simply infusing one principle or technique into another field, yet producing new achievements. For example, in comparison with AuNPs-based colorimetric assays, nanomaterials-based fluorescence analysis can be adapted from these assays in the following two aspects (Chinen et al., 2015; Lin et al., 2014; Yao et al., 2014). First, the nanoparticles-based fluorescent sensors show many intrinsic advantages over other optical methods such as high sensitivity, easy operation, and multiplicity of measurable parameters. Second, AuNPs can quench the fluorescence of fluorescent organic dyes and quantum dots (QDs) through the fluorescence resonance energy transfer (FRET) or the efficient inner filter effect (IFE) (Chang and Ho, 2015; Oh et al., 2005; Saha et al., 2012; Shamsipur et al., 2016; Xu et al., 2016; Xue et al., 2012; Yan et al., 2014; Zhang et al., 2012; Zhao et al., 2013). In particular, the IFE method does not require the intermolecular connection of fluorophores and absorbers at a particular distance, which provides a comparatively simple and facile approach for the analytical detection (Cao et al., 2014; Shang and Dong, 2009). Considering the unique optical properties of QDs and the high quenching efficiency of dispersed AuNPs on the fluorescence of QDs through the IFE (due to the complementary overlap between the surface plasmon resonance absorption of AuNPs and the emission fluorescence of QDs) (Yan et al., 2015; Zhang et al., 2015), herein, we developed a simple method for visual and fluorescent detection of AβOs. The proposed biosensor is specific for detection of AβOs but not for AβMs and AβFs, does not need to label peptide or modify AuNPs and QDs, and obviates the utilization of expensive and less stable antibody for recognition of AβOs.

2. Experimental

2.1. Chemicals and reagents

Aβ peptide with 42 amino acid residues ($Aβ_{1–42}$), bovine serum albumin (BSA), immunoglobin G (IgG), thrombin, cadmium chloride ($CdCl_2$), tellurium powder, sodium borohydride, glutathione (GSH), 1,1,1,3,3,3-hexafluoro-2-propanol (HFIP), KH_2PO_4 and K_2HPO_4 were purchased from Sigma-Aldrich. Trisodium citrate was obtained from Sangon Biotech. Co., Ltd. (Shanghai, China). PrP(95–110) peptide with a sequence of THSQWNKPSKPKTNMK was synthesized and purified by China-Peptides Co., Ltd. (Shanghai, China). The PrP(95–110) stock solution (1 mM) was prepared with deionized water and diluted with a phosphate-buffered saline solution (PBS buffer, 2 mM, pH 7.2) before use. All other chemicals were of analytical grade and obtained from Beijing Chemical Reagent Co. Ltd. (Beijing, China). All solutions were prepared with deionized water purified by using a Millipore system (Simplicity Plus, Millipore Corp.).

2.2. Syntheses of CdTe QDs

Water-soluble GSH-capped CdTe QDs were prepared according to the reported procedure with minor modifications (Li et al., 2013b). Fresh sodium hydrogen telluride (NaHTe) solution was made by dissolving sodium borohydride (25 mg) in 1 mL of deionized water, followed by addition of tellurium powder (40 mg). The mixed solution was heated at 60 °C for 40 min. The $CdCl_2$-GSH stock solution was prepared by dissolving $CdCl_2$ (14.3 mg) and GSH (16 mg) in 50 mL of deionized water, followed by adjusting the pH to 9.0 with a sodium hydroxide solution. For the preparation of GSH-capped CdTe QDs, 100 μL of the freshly prepared NaHTe solution was mixed with the $CdCl_2$-GSH stock solution. The mixed solution was boiled continually for 30 min and then cooled to room temperature. The whole synthetic process was carried out under N_2 atmosphere. For the purification of CdTe QDs, the resulting product was sealed in a dialysis membrane with a molecular weight of cutoff 8000, and the dialysis membrane was placed in a NaOH solution (0.01 M) for 2 days to remove the free $CdCl_2$ and GSH. The as-prepared CdTe QDs were diluted with a PBS solution (2 mM, pH 7.2) to 0.1 μM for use. The concentration of CdTe QDs was calculated according to the method reported previously (Yu et al., 2003). The prepared AuNPs was characterized by Dynamic light scattering (DLS) as shown in Fig. S1.

2.3. Synthesis of AuNPs

The citrate-stabilized AuNPs with a size of 13 nm were prepared using a trisodium citrate reduction method, as reported previously (Grabar et al., 1995). Briefly, trisodium citrate (5 mL, 38.8 mM) was rapidly added to a boiling solution of $HAuCl_4$ (50 mL, 1 mM), and the solution was boiled continually for an additional 30 min to yield a wine-red solution. DLS image of the prepared AuNPs was shown in Fig. S1. The concentration of AuNPs was calculated from the UV–vis absorption spectrum by using an extinction coefficient of $2.7 \times 10^8\ mol^{-1}\ cm^{-1}$ at 520 nm (Liu et al., 2014b). The citrate-stabilized AuNPs were diluted with the PBS solution (2 mM, pH 7.2) for use. Note that all glassware used in the preparation procedure was cleaned in a bath of freshly prepared HNO_3–HCl (v/v=1/3), rinsed thoroughly with water and dried in air prior to use.

2.4. Preparation of soluble AβOs

Soluble AβOs were prepared as in the previous reports (Laurén et al., 2009; Liu et al., 2015). Briefly, $Aβ_{1–42}$ lyophilized powder was

first dissolved in HFIP at a concentration of 1 mg/mL and sonicated for 10 min to monomerize pre-existing aggregates. After HFIP was evaporated under a gentle stream of high purity nitrogen, the resulting $A\beta_{1-42}$ was reconstituted in 20 mM NaOH to a concentration of 2 mM, and then diluted to a final concentration of 50 μM with a phosphate-buffered saline solution (PBS buffer, 10 mM, pH 7.2). After incubation at 25 °C for a given time, the sample was used for experiments. The peptide concentration was determined by the UV–vis spectra with an extinction coefficient of 1410 M^{-1} cm^{-1} at 276 nm. The concentrations of AβOs in this study are calculated as equivalent concentrations to monomers.

The Aβ species at different forms were characterized by Atomic Force Microscopy (AFM) with a Dimension Edge microscope (Bruker Nano Inc., Santa Barbara, CA) equipped with a tapping mode. Briefly, aliquots of $A\beta_{1-42}$ at the concentration of 50 μM were taken out at predetermined incubation times, cast onto newly peeled mica, and left in contact with the mica substrate for 15 min. The slides were washed with water to remove any residual salt, and dried under a very gentle nitrogen stream before imaging.

2.5. Quenching efficiency of dispersed AuNPs on CdTe QDs

To investigate the fluorescence quenching ability of AuNPs toward CdTe QDs, 200 μL of different concentrations of AuNPs suspensions were added to 200 μL of 0.1 μM CdTe QDs solution. Fluorescence spectra were then taken with a Varian Cary fluorescence spectrometer upon excitation at 370 nm. The emission wavelengths were collected with both excitation and emission slits of 5 nm.

2.6. Colorimetric assays for PrP(95–110)-triggered AuNPs aggregation

To investigate the effect of PrP(95–110) concentration on the aggregation of AuNPs, 500 μL of AuNPs dispersion at a given concentration was added to 500 μL of different concentration of PrP(95–110) solution. After incubation for 5 min, color change and UV–vis absorption spectra were observed with the naked eyes and recorded with a Cary 50 spectrophotometer using a 1 cm quartz spectrophotometer cell, respectively. The photographs were taken with a Sony Cyber-shot digital camera.

2.7. AβOs detection

240 μL of PrP(95–110) solutions was first mixed with 10 μL of different concentrations of AβOs in the test tubes for 5 min. Then, the mixture was incubated with 750 μL of AuNPs at room temperature for 5 min. Then, the color change and absorption spectra of the mixture solutions were recorded by the digital camera and the UV–vis spectrophotometer. For fluorescence assays, 200 μL of CdTe QDs were added to 200 μL of the above sample solutions. After reaction for 1 min, the emission spectroscopy measurements were recorded with the excitation wavelength at 370 nm.

3. Results and discussion

3.1. Principle of the visual and fluorescent assay

In this work, GSH-capped CdTe QDs were used as the fluorophores since their fluorescence emission shows good complementary overlap with the surface plasmon resonance absorption of dispersed AuNPs, thus allowing for the occurrence of the IFE between AuNPs and QDs (Li et al., 2013b). The principle of the proposed visual and fluorescent assays is illustrated in Fig. 1. The fluorescence emission of CdTe QDs was quenched significantly by AuNPs through the IFE. The AβOs-specific binding peptide (PrP (95–110), THSQWNKPSKPKTNMK) could adsorb onto the surface of AuNPs, thus triggering the aggregation and color change of AuNPs suspension. As a result, the IFE of AuNPs on the fluorescence of CdTe QDs was weakened and the fluorescence intensity was recovered. Upon addition of Aβ sample to the PrP(95–110) solution, PrP(95–110) interacted specifically with AβOs, thus losing the capability to induce the aggregation of AuNPs. This method offers high simplicity because it obviates the need of modified receptors and does not require the modification of AuNPs and CdTe QDs.

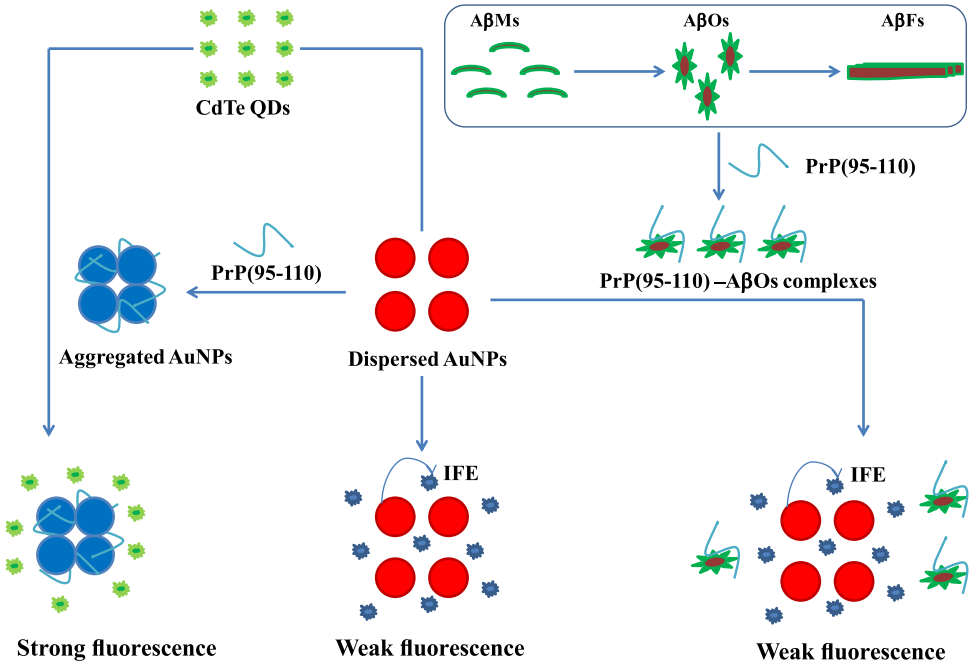

Fig. 1. Schematic illustration of the visual and fluorescent detection of AβOs through the IFE of AuNPs on the fluorescence of CdTe QDs.

3.2. Feasibility for visual and fluorescent assays of AβOs

Aβ species at different aggregation states were characterized by AFM, as shown in Fig. 2(A). To demonstrate the feasibility of this method, PrP(95–110)-triggered color and absorbance changes of AuNPs suspension in the absence and presence of different aggregation states of Aβ were first investigated by naked eyes and UV–vis spectrophotometer. As shown in Fig. 2(B), the red AuNPs solution exhibited an absorption peak at 520 nm (tube a and curve a), which was ascribed to the surface plasmon resonance absorption of AuNPs. Upon the addition of PrP(95–110), the color of AuNPs suspension changed from red to blue (tube b). Meanwhile, the original absorbance of AuNPs suspension at 520 nm decreased while a new absorbance peak at around 650 nm increased obviously (cf. curve a and curve b), indicating that the aggregation of AuNPs was induced by PrP(95–110). The result is understandable since PrP(95–110) contains four positively charged lysine residues and no negatively charged amino-acid residue is included in the sequence. So it was readily adsorbed onto the surface of negatively charged AuNPs through the electrostatic interaction. Among the cases of AβMs (curve c), AβOs (curve d) and AβFs (curve e), only in the presence of AβOs the color of AuNPs remained red and one absorption peak at 520 nm was observed. This result was further confirmed by transmission electron microscope (TEM) observations: significant aggregation of AuNPs in the presence of PrP(95–110) alone and monodisperse of AuNPs in the presence of PrP(95–110)/AβOs (Fig. S2). Note that Aβ itself at the three states did not cause the obvious changes in the color and absorbance of AuNPs suspension (data not shown). Thus, the inhibition of PrP (95–110)-triggered AuNPs aggregation was contributed to the specific interaction between PrP(95–110) and AβOs. The result also confirmed that the secondary structure of Aβ is indispensable for the recognition of PrP(95–110). Furthermore, although the CdTe QDs shows an absorption maximum at 477 nm, no obvious changes in the absorption spectrum of AuNPs were observed in the presence of 0.05 μM CdTe QDs. The result is acceptable since there is no interaction between citrate-stabilized AuNPs and GSH-capped CdTe QDs (Li et al., 2013b).

Fig. 2(C) shows the fluorescence spectra of CdTe QDs in the absence and presence of different states of AuNPs. To demonstrate the feasibility of the fluorescence assay, we first investigated the effect of PrP(95–110) and AβOs on the fluorescence intensity and found that PrP(95–110), AβOs or PrP(95–110)-AβOs themselves did not cause apparent change in the fluorescence spectra of CdTe QDs (cf. curve a and curve b). However, AuNPs in the dispersed states resulted in a reduction of ~68% in the fluorescence intensity of CdTe QDs (curves c and e), but the aggregated AuNPs only caused a decrease in the fluorescence intensity by ~26% (curves d, f and g).

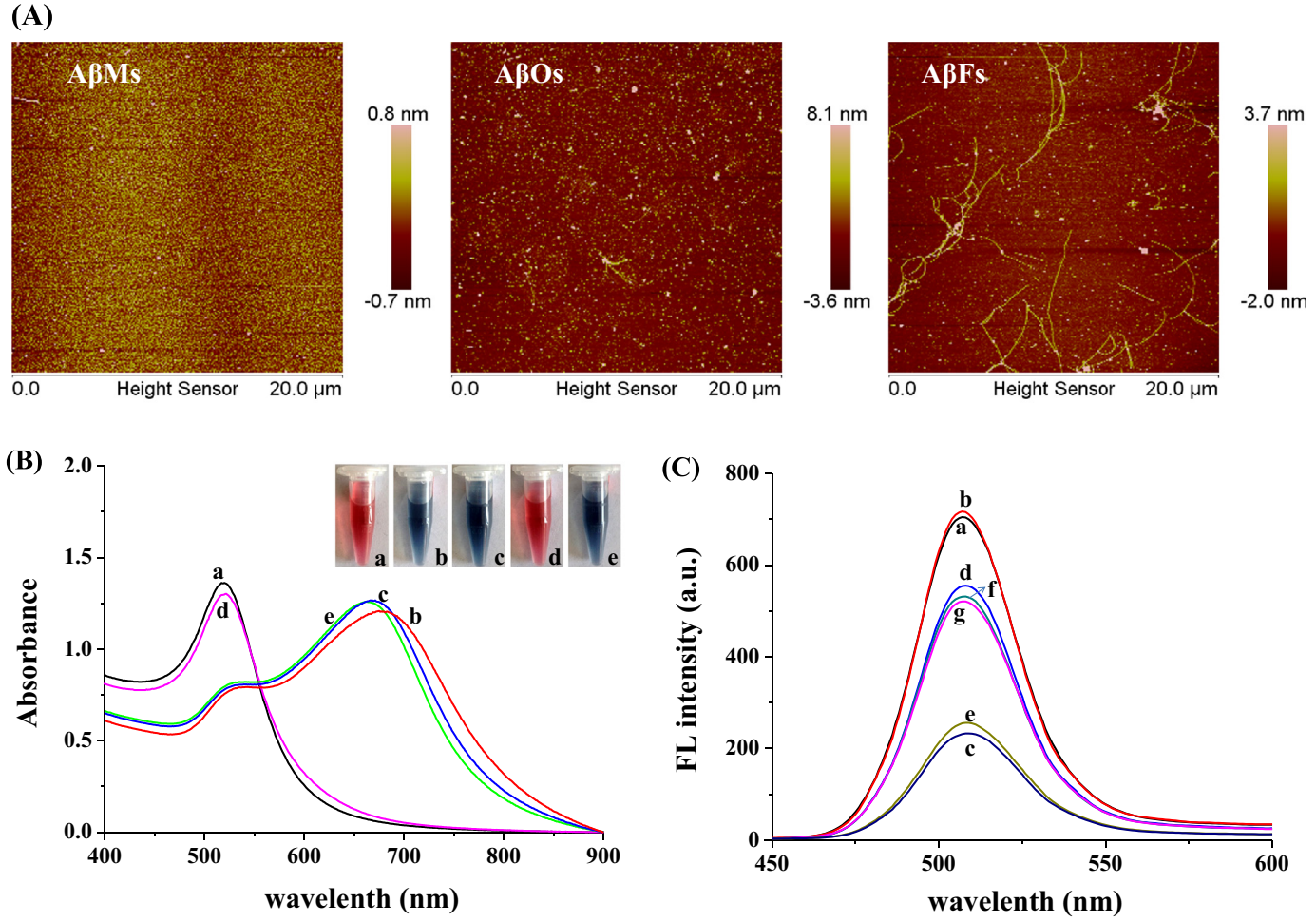

Fig. 2. (A) Atomic force microscopy (AFM) images of the mica substrates after incubation with AβMs, AβOs and AβFs. (B) UV–vis absorption spectra of AuNPs in various systems (a, AuNPs; b, AuNPs/PrP(95–110); c, AuNPs/PrP(95–110)/AβMs; d, AuNPs/PrP(95–110)/AβOs; e, AuNPs/PrP(95–110)/AβFs). The final concentrations of AuNPs, PrP(95–110) and Aβ samples are 5 nM, 0.2 μM and 5 μM, respectively. The inset shows the photographic images of AuNPs in the dispersed and aggregated states. (C) Fluorescence spectra of CdTe QDs in various systems (a, CdTe; b, CdTe/PrP(95–110); c, CdTe/AuNPs; d, CdTe/AuNPs/PrP(95–110); e, CdTe/AuNPs/PrP(95–110)/AβOs; f, CdTe/AuNPs/PrP(95–110)/AβMs; g, CdTe/AuNPs/PrP(95–110)/AβFs). The final concentrations of CdTe, AuNPs, PrP(95–110) and Aβ samples are 0.05 μM, 2.5 nM, 0.1 μM and 2.5 μM, respectively. (For interpretation of the references to color in this figure, the reader is referred to the web version of this article.)

The results are understandable since the IFE occurs effectively only if the absorption band of the absorber possesses a complementary overlap with the excitation and/or emission bands of the fluorophore (Shang and Dong, 2009), and the absorption spectrum of the dispersed but not aggregated AuNPs overlaps very well with the fluorescence emission spectrum of CdTe QDs at 508 nm. Additionally, the reduction of the fluorescence intensity in the curves d, f and g (compared with curve a) could be attributed to the existence of less amount of dispersed AuNPs in the solution (cf. the absorption at 520 nM in curves b, c and e of Fig. 2(B)). Overall, these results indicated that the change in the absorbance of the absorber can translate into exponential change in fluorescence of the fluorophore, and that both the UV–vis and fluorescence signal responses are specific to AβOs but not for AβMs and AβFs.

3.3. Optimization of experimental conditions

As depicted in Fig. 2(B) and (C), the good overlap of the absorption band of AuNPs with the phosphorescence emission band of CdTe QDs provides a precondition for the IFE between AuNPs and QDs. To demonstrate the generality of our design using AuNPs as an IFE-absorber and CdTe QDs as an IFE-fluorophore for AβOs detection, a series of experimental conditions were optimized. First, we noticed that the concentration of CdTe QDs used herein was in an optimal linear range of fluorescence intensity-concentration; thus, CdTe QDs at a final concentration of 0.05 μM was used in the following experiments. The fluorescence spectra of CdTe QDs were then recorded when the QDs were mixed with various concentrations of AuNPs. It can be observed that the fluorescence emission gradually decreases upon increasing concentrations of AuNPs and trends to a minimum value beyond 1.25 nM AuNPs (Fig. 3(A)). The quenching efficiency of AuNPs for QDs was calculated using the formula $(1-F/F_0)\times 100\%$ to be 65% ± 2.4%, where F_0 and F are the fluorescence intensities at 508 nm in the absence and presence of AuNPs, respectively. When the concentration of AuNPs increased to 2.5 nM, more than 68% of the fluorescence emission from CdTe QDs (0.05 μM) was quenched. Although higher concentration of AuNPs can make the fluorescence quenching of CdTe QDs more powerful, higher concentration of AuNPs requires higher concentration of PrP(95–110) and AβOs, which would deteriorate the assay cost and sensitivity. Thus, in this work, AuNPs suspension at a final concentration of 1.25 (or 2.5 nM) was chosen for the fluorescent (or visual) assay.

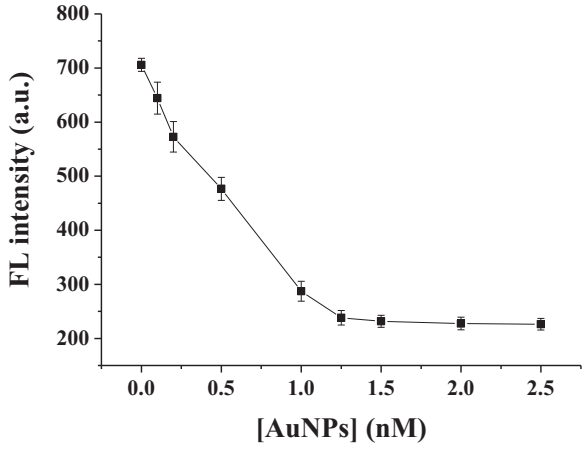

Fig. 3. Quenching efficiency of different concentrations of AuNPs (0, 0.1, 0.2, 0.5, 1, 1.25, 1.5, 2 and 2.5 nM) for 0.05 μM QDs.

Concentration of PrP(95–110) and incubation time for AβOs preparation also have a significant influence on the visual and fluorescent assays. Firstly, the concentration of PrP(95–110) was examined in the range from 0 to 100 nM by UV–vis spectrophotometer. The results showed that the A_{650}/A_{520} ratio (wherein A_{650} and A_{520} represent the absorption intensity of the solutions at 650 nm and 520 nm, respectively) increased linearly with the increase of PrP(95–110) concentration in the range of 1–60 nM and began to level off beyond 60 nM (Fig. 4(A)). Thus, in the further experiment 60 nM PrP(95–110) was used. The effect of incubation time for AβOs preparation on inhibition of PrP(95–110)-triggered color and absorbance changes of AuNPs was also studied. Herein, the A_{520}/A_{650} ratio was used to evaluate to analytical performances of the visual assay. We found that the A_{520}/A_{650} ratio reaches to the maximum for 30 h incubation, indicating that the optimal incubation time for AβOs formation was around 30 h (Fig. 4(B)). Thus, in the following detection assays, 30 h was set as the standard condition for AβOs preparation.

3.4. Sensitivity

As shown in the inset of Fig. 5(A), the color of the AuNPs suspension changed from blue to red gradually in the presence of a given concentration of PrP(95–110) and increasing concentration of AβOs. The result further demonstrated that AβOs prevented the PrP(95–110)-triggered aggregation of AuNPs. The visible color change could be easily distinguished by naked eyes from the blank test (without AβOs) when the target concentration was over

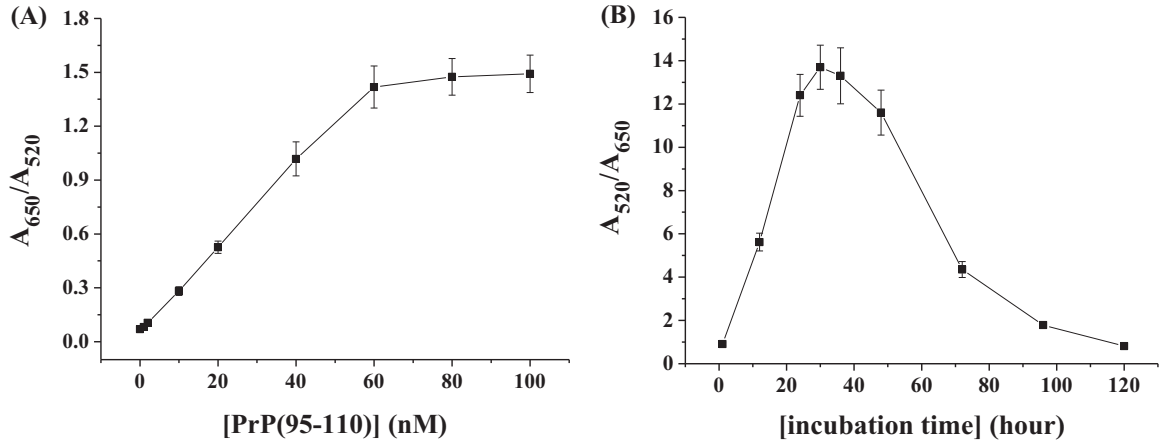

Fig. 4. Effect of PrP(95–110) concentration (A) and incubation time for AβOs formation (B) on the relative UV–vis absorption intensity change of AuNPs. The concentration of AuNPs is 2.5 nM and the final concentrations of PrP(95–110) and Aβ samples in panel B are 60 nM and 2.5 μM, respectively.

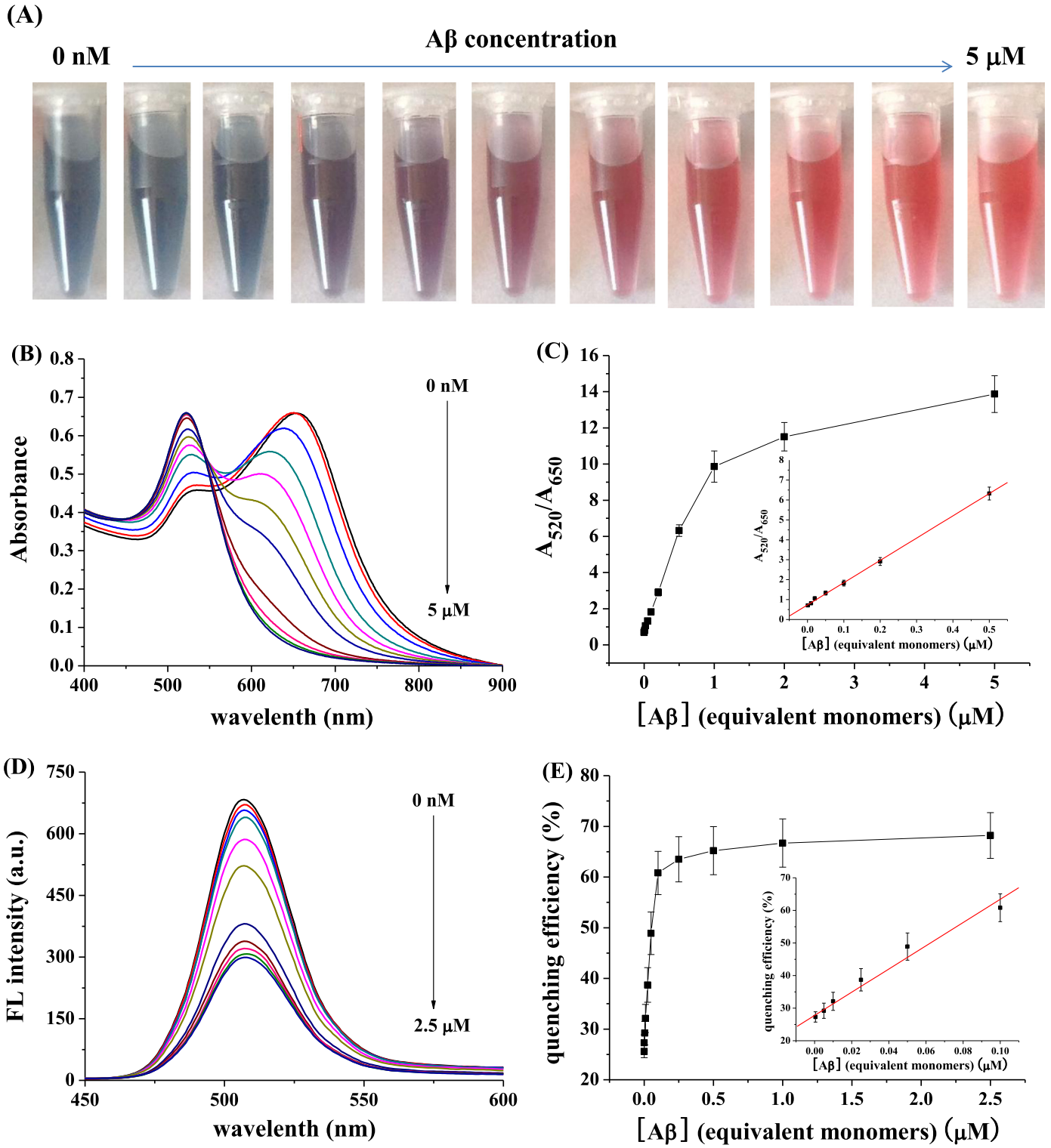

Fig. 5. Photographic images (A) and UV–vis absorption spectra (B) of 2.5 nM AuNPs in the presence of 60 nM PrP(95–110) and different concentrations of AβOs (equivalent monomers: 0, 0.001, 0.01, 0.02, 0.05, 0.1, 0.2, 0.5, 1, 2 and 5 μM). (C) Dependence of the A_{520}/A_{650} ratio on the Aβ concentration. (D) Fluorescence spectra of 0.05 μM CdTe QDs in the presence of 1.25 nM AuNPs, 30 nM PrP(95–110) and different concentrations of AβOs (equivalent monomers: 0, 0.0005, 0.005, 0.01, 0.025, 0.05, 0.1, 0.25, 0.5, 1 and 2.5 μM). (E) Dependence of the quenching efficiency on the Aβ concentration. (For interpretation of the references to color in this figure, the reader is referred to the web version of this article.)

20 nM, that is to say, the colorimetric assay allows for AβOs detection at a concentration as low as 20 nM for a rapid and reliable visualization of AβOs by comparison with the AβOs-free blank sample. The UV–vis spectra investigations also revealed that the red-shifted band corresponding to the aggregated AuNPs was decreased by increasing the AβOs concentration from 0 to 5 μM, which was accompanied by an increase of absorbance at 520 nm (Fig. 5(B)). A good linear relationship between the A_{520}/A_{650} and the concentration of AβOs (equivalent monomers) was obtained in the range from 1 nM to 0.5 μM (Fig. 5(C)). The regression equation is $A_{520}/A_{650}=0.73+11.18$ [Aβ] (μM) ($R^2=0.99$). The detection limit was estimated to be 0.5 nM ($n=11$) for the equivalent monomers.

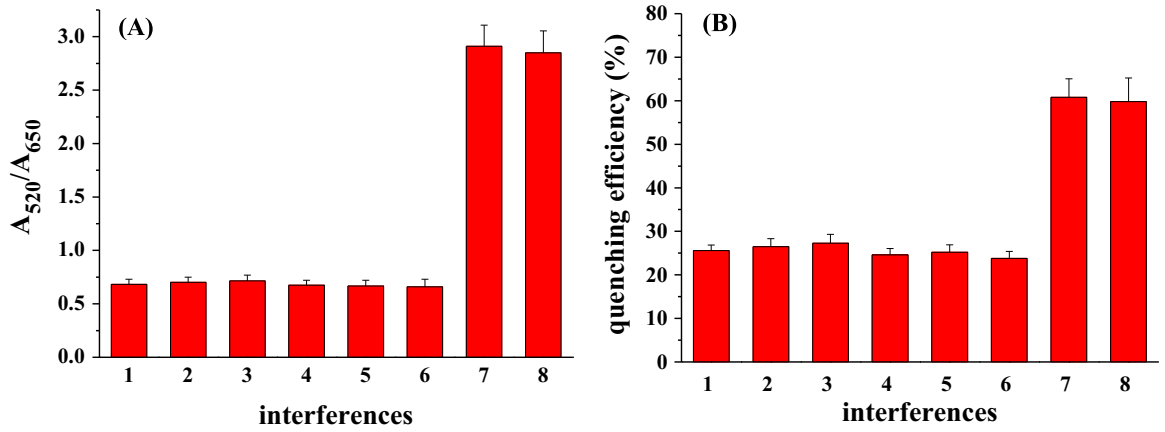

Fig. 6. Selectivity and interference of the sensing protocol. From bar 1 to bar 8: control, AβMs, AβFs, BSA, IgG, thrombin, AβOs, and AβOs/AβMs/AβFs/interferences. The final concentrations of Aβ and interferences are 0.2 μM in panel A and 0.1 μM in panel B. The other experimental conditions are the same as those in Fig. 5.

As mentioned above, upon the addition of AβOs the aggregation of AuNPs caused by PrP(95–110) was prevented; thus, the efficiency of the IFE was enhanced. We also found that the fluorescence intensity of CdTe QDs was continuously reduced with the increase of AβOs concentration in the range of 0.5 nM–2.5 μM (Fig. 5(D)). The fluorescence data were analyzed by plotting the fluorescence quenching efficiency $(1-F_1/F_0)\times 100\%$ versus the concentration of AβOs (equivalent monomers) (F_0 and F_1 are the fluorescence intensity of the CdTe QDs in the absence and presence of AuNPs/PrP (95–110)/AβOs, respectively). It can be observed that the quenching efficiency increased linearly with the increasing concentration of AβOs ranging from 0.5 nM to 0.1 μM and begins to level off beyond 0.25 μM (Fig. 5(E)). The linear regression equation is $Y\% = 356.5\ [A\beta]\,(\mu M) + 27.8$ ($R^2 = 0.99$). The detection limit of the fluorescent method was estimated to be 0.2 nM (n=11) for the equivalent monomers. This value is comparable to that obtained by molecular beacon (MB)-based fluorescent assay (3.57 nM) (Zhu et al., 2016), square wave voltammetry (48 pM) (Li et al., 2013a), cyclic voltammetry by signal amplification of electrochemical–chemical–chemical redox cycling (3 pM) (Liu et al., 2015), electrochemical impedance spectroscopy (100 pM) (Rushworth et al., 2014), magnetic bead-droplet immunoassay (10 mg mL^{-1}) (Kim et al., 2015), localized surface plasmon resonance (LSPR) (0.1 pM) (Haes et al., 2005) and AuNPs-based LSPR (1.5 pM) (Kang et al., 2015). However, our method exhibits excellent selectivity to AβOs, does not need to label peptide or modify AuNPs and QDs, requires very simple sample handling, and obviates the utilization of expensive and less stable antibody, which improves the detection specificity and reduces the operation complexity, analysis time and detection cost. Moreover, the direct visualization of AβOs by naked eyes obviates the need of special equipment. In addition, although the organic dyes-based fluorescence assays (e.g. thioflavin T or ThT) have been commonly used for monitoring the formation of Aβ aggregates in laboratory investigations (Amaro et al., 2010; Arosio et al., 2014; Ren et al., 2016). However, most of the dyes cannot be used to discriminate AβOs from other β-sheets of Aβ aggregates. Thus, our method may offer a useful means for quantifying AβOs in other types of laboratory studies (e.g., probing of the dynamics and mechanism of Aβ aggregation/fibrillation processes under different experimental conditions and screening of novel inhibitors that can prevent the formation of neurotoxic AβOs).

3.5. Selectivity and interference

To explore the specificity of the proposed method, AβMs, AβFs and three interfering proteins (BSA, IgG and thrombin) were chosen for the selectivity and interference studies. As shown in Fig. 6, compared to the control (bar 1), all of these interferences did not cause significant changes in both A_{520}/A_{650} and fluorescence quenching efficiency (bars 2–6). The results confirmed that the established visual and IFE-based fluorescent assays show extraordinary selectivity towards AβOs. The high selectivity could be principally attributed to the strong and specific interaction between PrP(95–110) and AβOs. To further investigate the interference, AβMs, AβFs and these three interfering proteins were collectively incubated with AβOs for 2 min before the addition of PrP(95–110). We found that addition of these interferences to the AβOs solution has no meaningful impact on the A_{520}/A_{650} ratio and the quenching efficiency (bar 8) in comparison with that in the presence of AβOs only (bar 7). These results are indicative of the potential applicability of the sensing protocol for AβOs detection in biological matrix samples.

4. Conclusion

In summary, we reported a label-free strategy for visual and fluorescent detection of AβOs based on the IFE of AuNPs on the fluorescence of CdTe QDs. The method has good sensitivity and enables accurate quantification of AβOs as low as 0.5 nM by UV–vis spectra and 0.2 nM by fluorescence. Compared with other methods for AβOs detection such as immunoassay, LSPR and electrochemistry, our method shows several analytical advantages. First, it exhibits excellent selectivity to AβOs but not for AβMs and AβFs because of the specific recognition of PrP(95–110) to AβOs. Second, the strategy does not need to label peptide or modify AuNPs and QDs, reducing the operation complexity, analysis time and detection cost. Third, it obviates the utilization of expensive and less stable antibody for recognition of AβOs. Fourthly, the direct visualization of AβOs (below 20 nM) by naked eyes requires very simple sample handling procedure and minimum instrumental investment, which may offer a useful means for quantifying AβOs in other types of laboratory studies (e.g., probing of the dynamics and mechanism of Aβ aggregation/fibrillation processes under different experimental conditions and screening of novel inhibitors that can prevent the formation of neurotoxic AβOs). Moreover, because direct assay of soluble AβOs would be more reliable for early diagnosis of AD than assay of AβMs, the proposed biosensor could potentially serve as a viable alternative for facile and sensitive clinical analysis of Aβ species related to AD diagnosis.

Acknowledgments

Partial support of this work by the National Natural Science Foundation of China (Nos. 21205003 and 21305004), the Joint Fund for Fostering Talents of National Natural Science Foundation of China and Henan Province (U1304205) and the Program for Science and Technology Innovation Talents at the University of Henan Province (15HASTIT001) is gratefully acknowledged.

Appendix A. Supplementary material

Supplementary data associated with this article can be found in the online version at http://dx.doi.org/10.1016/j.bios.2016.05.066.

References

Amaro, M., Birch, D.J.S., Rolinski, O.J., 2010. Biosens. Bioelectron. 25, 2249–2252.
Arosio, P., Cukalevski, R., Frohm, B., Knowles, T.P.J., Linse, S., 2014. J. Am. Chem. Soc. 136, 219–225.
Balducci, C., Beeg, M., Stravalaci, M., Bastone, A., Sclip, A., Biasini, E., Tapella, L., Colombo, L., Manzoni, C., Borsello, T., Chiesa, R., Gobbi, M., Salmona, M., Forloni, G., 2010. Proc. Nat. Acad. Sci. USA 107, 2295–2300.
Cao, X., Shen, F., Zhang, M., Sun, C., 2014. Sens. Actuators B: Chem. 202, 1175–1182.
Chang, H.C., Ho, J.A.A., 2015. Anal. Chem. 87, 10362–10367.
Chen, S., Yadav, S.P., Surewicz, W.K., 2010. J. Biol. Chem. 285, 26377–26383.
Chinen, A.B., Guan, C.M., Ferrer, J.R., Barnaby, S.N., Merkel, T.J., Mirkin, C.A., 2015. Chem. Rev. 115, 10530–10574.
Elghanian, R., Storhoff, J.J., Mucic, R.C., Letsinger, R.L., Mirkin, C.A., 1997. Science 277, 1078–1081.
Escosura-Muñiz, A., Plichta, Z., Horák, D., Merkoçi, A., 2015. Biosens. Bioelectron. 67, 162–169.
Fluharty, B.R., Biasini, E., Stravalaci, M., Sclip, A., Diomede, L., Balducci, C., Vitola, P.L., Messa, M., Colombo, L., Forloni, G., Borsello, T., Gobbi, M., Harris, D.A., 2013. J. Biol. Chem. 288, 7857–7866.
Freir, D.B., Nicoll, A.J., Klyubin, I., Panico, S., Donald, J.M.M., Risse, E., Asante, E.A., Farrow, M.A., Sessions, R.B., Saibil, H.R., Clarke, A.R., Rowan, M.J., Walsh, D.M., Collinge, J., 2011. Nat. Commun. 2, 1–9.
Gagni, P., Sola, L., Cretich, M., Chiari, M., 2013. Biosens. Bioelectron. 47, 490–495.
Glabe, C.G., 2008. J. Biol. Chem. 283, 29639–29643.
Golde, T.E., Eckman, C.B., Younkin, S.G., 2000. Biochim. Biophys. Acta 1502, 172–187.
Grabar, K.C., Freeman, R.G., Hommer, M.B., Natan, M.J., 1995. Anal. Chem. 67, 735–743.
Guillot-Sestier, M.V., Sunyach, C., Ferreira, S.T., Marzolo, M.P., Bauer, C., Thevenet, A., Checler, F., 2012. J. Biol. Chem. 287, 5021–5032.
Haes, A.J., Chang, L., Klein, W.L., Van Duyne, R.P., 2005. J. Am. Chem. Soc. 127, 2264–2271.
Kang, M.K., Lee, J., Nguyen, A.H., Sim, S.J., 2015. Biosens. Bioelectron. 72, 197–204.
Kaushik, A., Jayant, R.D., Tiwari, S., Vashist, A., Nair, M., 2016. Biosens. Bioelectron. 80, 273–287.
Kim, J.A., Kim, M., Kang, S.M., Lim, K.T., Kim, T.S., Kang, J.Y., 2015. Biosens. Bioelectron. 67, 724–732.
Laurén, J., Gimbel, D.A., Nygaard, H.B., Gilbert, J.W., Strittmatter, S.M., 2009. Nature 457, 1128–1132.
Li, H., Xie, H., Cao, Y., Ding, X., Yin, Y., Li, G., 2013a. Anal. Chem. 85, 1047–1052.
Li, J., Li, X., Shi, X., He, X., Wei, W., Ma, N., Chen, H., 2013b. ACS Appl. Mater. Interfaces 5, 9798–9802.
Lin, L., Rong, M., Luo, F., Chen, D., Wang, Y., Chen, X., 2014. TrAC-Trends Anal. Chem. 54, 83–102.
Liu, L., He, Q., Zhao, F., Xia, N., Liu, H., Li, S., Liu, R., Zhang, H., 2014a. Biosens. Bioelectron. 51, 208–212.
Liu, L., Li, S., Liu, L., Deng, D., Xia, N., 2012. Analyst 137, 3794–3799.
Liu, L., Xia, N., Jiang, M., Huang, N., Guo, S., Li, S., Zhang, S., 2015. J. Electroanal. Chem. 754, 40–45.
Liu, L., Xia, N., Liu, H., Kang, X., Liu, X., Xue, C., He, X., 2014b. Biosens. Bioelectron. 53, 399–405.
Liu, L., Zhao, F., Ma, F., Zhang, L., Yang, S., Xia, N., 2013. Biosens. Bioelectron. 49, 231–235.
Oh, E., Hong, M.Y., Lee, D., Nam, S.H., Yoon, H.C., Kim, H.S., 2005. J. Am. Chem. Soc. 127, 3270–3271.
Rauk, A., 2009. Chem. Soc. Rev. 38, 2698–2715.
Reinke, A.A., Ung, P.M.U., Quintero, J.J., Carlson, H.A., Gestwicki, J.E., 2010. J. Am. Chem. Soc. 132, 17655–17657.
Ren, W., Xu, M., Liang, S.H., Xiang, H., Tang, L., Zhang, M., Ding, D., Li, X., Zhang, H., Hu, Y., 2016. Biosens. Bioelectron. 75, 136–141.
Rushworth, J.V., Ahmed, A., Griffiths, H.H., Pollock, N.M., Hooper, N.M., Millner, P.A., 2014. Biosens. Bioelectron. 56, 83–90.
Saha, K., Agasti, S.S., Kim, C., Li, X.N., Rotello, V.M., 2012. Chem. Rev. 112, 2739–2779.
Selkoe, D.J., 2008. Behav. Brain Res. 192, 106–113.
Shamsipur, M., Memari, Z., Ganjali, M.R., Norouzi, P., Faridbod, F., 2016. J. Pharm. Biomed. Anal. 118, 356–362.
Shang, L., Dong, S., 2009. Anal. Chem. 81, 1465–1470.
Walsh, D.M., Klyubin, I., Fadeeva, J.V., Cullen, W.K., Anwyl, R., Wolfe, M.S., Rowan, M. J., Selkoe, D.J., 2002. Nature 416, 535–539.
Wang, C., Liu, D., Wang, Z., 2011. Chem. Commun. 47, 9339–9341.
Wang, C., Liu, D., Wang, Z., 2012. Chem. Commun. 48, 8392–8394.
Xia, N., Liu, L., Harrington, M.G., Wang, J.X., Zhou, F.M., 2010. Anal. Chem. 82, 10151–10157.
Xing, Y., Xia, N., 2015. Anal. Lett. 48, 879–893.
Xu, J., Yu, H., Hu, Y., Chen, M.Z., Shao, S.J., 2016. Biosens. Bioelectron. 75, 1–7.
Xue, M., Wang, X., Duan, L., Gao, W., Ji, L., Tang, B., 2012. Biosens. Bioelectron. 36, 168–173.
Yan, X., Li, H., Li, Y., Su, X., 2014. Anal. Chim. Acta 852, 189–195.
Yan, X., Li, H.X., Han, X.S., Su, X.G., 2015. Biosens. Bioelectron. 74, 277–283.
Yao, J., Yang, M., Duan, Y., 2014. Chem. Rev. 114, 6130–6178.
Yu, W.W., Qu, L., Guo, W., Peng, X., 2003. Chem. Mater. 15, 2854–2860.
Yu, Y., Sun, X., Tang, D., Li, C., Zhang, L., Nie, D., Yin, X., Shi, G., 2015. Biosens. Bioelectron. 68, 115–121.
Yu, Y.Y., Zhang, L., Li, C.L., Sun, X.Y., Tang, D.Q., Shi, G.Y., 2014. Angew. Chem. Int. Ed. 53, 12832–12835.
Zhang, M., Cao, X., Li, H., Guan, F., Guo, J., Shen, F., Luo, Y., Sun, C., Zhang, L., 2012. Food Chem. 135, 1894–1900.
Zhang, R., Li, N., Sun, J., Gao, F., 2015. J. Agric. Food Chem. 63, 8947–8954.
Zhao, J., Yi, Y., Mi, N., Yin, B., Wei, M., Chen, Q., Li, H., Zhang, Y., Yao, S., 2013. Talanta 116, 951–957.
Zhu, L., Zhang, J., Wang, F., Wang, Y., Lu, L., Feng, C., Xu, Z., Zhang, W., 2016. Biosens. Bioelectron. 78, 206–212.